AD-A262 178

ARMY RESEARCH LABORATORY

Numerical Simulation of Fluid Dynamics and Payload Dissemination in a Dual-Chamber Grenade

Michael J. Nusca

ARL-TR-77

February 1993

NOTICES

REPORT DOCUMENTATION PAGE

Form Approved
OMB No. 0704-0188

1. AGENCY USE ONLY *(Leave blank)*

2. REPORT DATE
February 1993

3. REPORT TYPE AND DATES COVERED
Final June 1991 - January 1992

4. TITLE AND SUBTITLE
Numerical Simulation of Fluid Dynamics and Payload Dissemination in a Dual-Chamber Grenade

5. FUNDING NUMBERS
PR: 1L162618AH80

6. AUTHOR(S)
Michael J. Nusca

7. PERFORMING ORGANIZATION NAME(S) AND ADDRESS(ES)

8. PERFORMING ORGANIZATION REPORT NUMBER

9. SPONSORING/MONITORING AGENCY NAMES(S) AND ADDRESS(ES)
US Army Research Laboratory
ATTN: AMSRL-OP-CI-B (Tech Lib)
Aberdeen Proving Ground, MD 21005-5066

10. SPONSORING/MONITORING AGENCY REPORT NUMBER
ARL-TR-77

11. SUPPLEMENTARY NOTES

12a. DISTRIBUTION/AVAILABILITY STATEMENT
Approved for Public Release - Distribution is Unlimited

12b. DISTRIBUTION CODE

13. ABSTRACT *(Maximum 200 words)*

The internal design of a grenade used for the thermal dissemination of solid payload into the atmosphere can consist of two concentric cylinders - a pyrotechnic device in the outer annulus and payload material bonded to the wall of the inner cylinder. The two chambers are connected. Combustion of the pyrotechnic produces high pressure within the grenade. A pressure difference between the atmosphere and inside the grenade induces a through-flow that thermally erodes and vaporizes the material in the inner chamber. This material in gaseous form is entrained in this flow and expelled from the grenade. Payload dissemination can be simulated using computational fluid dynamics to solve the Navier-Stokes equations along with chemical species conservation equations. The pyrotechnic combustion is not modeled. Using chamber dimensions and payload chemical properties, this simulation yields velocity, pressure, temperature, density, and chemical composition of the gas in the inner chamber and exiting the grenade. Numerical simulations can aid in understanding the physics of dissemination and be used to conduct parametric design studies.

14. SUBJECT TERMS
fluid dynamics, boundary layer, Navier-Stokes equations, reacting flow

15. NUMBER OF PAGES
34

16. PRICE CODE

17. SECURITY CLASSIFICATION OF REPORT	18. SECURITY CLASSIFICATION OF THIS PAGE	19. SECURITY CLASSIFICATION OF ABSTRACT	20. LIMITATION OF ABSTRACT
UNCLASSIFIED	UNCLASSIFIED	UNCLASSIFIED	SAR

NSN 7540-01-280-5500

Standard Form 298 (Rev. 2-89)
Prescribed by ANSI Std. Z39-18
298-102

INTENTIONALLY LEFT BLANK.

TABLE OF CONTENTS

INTENTIONALLY LEFT BLANK.

LIST OF FIGURES

INTENTIONALLY LEFT BLANK.

Acknowledgment

This work was supported by Mr. Miles C. Miller of the Aerodynamics Research and Concepts Assistance (ARCA) Branch, Physics Division, Research Directorate, U.S. Army Chemical Research, Development, and Engineering Center (CRDEC), Aberdeen Proving Ground, MD.

INTENTIONALLY LEFT BLANK.

1. INTRODUCTION

The dissemination of solid payload material as a gaseous cloud from a container can be accomplished using a pressurized system (e.g. compressed CO_2 cartridge), a mechanical system (e.g. plunger) or a pyrotechnic system (e.g. central burster or hot/cold gas flow). In the latter technique, dissemination of the payload is realized after ablation and vaporization of the material from exposure to the thermal effects of pyrotechnic combustion. Experimental programs at the U.S. Army Chemical Research Development and Engineering Center (CRDEC) are being used to test the efficiency of the thermal/ablation method. The goals are high rate of dissemination and low temperature/high payload concentration in the dissemination cloud. These tests can involve highly instrumented full-scale and small-scale grenade models ignited within large test chambers. Numerical simulation in support of such tests was conducted at the U.S. Army Research Laboratory (ARL). These simulations are required to aid in data reduction, contribute to the physical understanding of thermal dissemination, and conduct parametric studies that may guide future tests.

The internal design of a grenade used for the thermal dissemination of solid payload into the atmosphere can consist of two concentric cylinders; a pyrotechnic device in the outer annulus and payload material bonded to the wall of the inner cylinder. The two chambers are connected. Combustion of the pyrotechnic produces a high pressure within the grenade. A pressure difference between the atmosphere and inside the grenade induces a thru-flow that thermally erodes and vaporizes the material in the inner chamber. The material in gaseous form is entrained in this flow and expelled from the grenade. Figure 1 shows the internal schematic of a generic grenade configuration.

Numerical simulation of the fluid dynamics associated with payload dissemination from a grenade is accomplished in the present study using the Navier-Stokes equations along with equations that govern chemical species ablation and diffusion. Chemical reactions between payload and pyrotechnic gases may be but are are not necessarily involved. An implicit finite-difference scheme based on successive-over-relaxation is used to solve these equations for the physical domain of interest. This domain resides within the inner chamber of the grenade; thus, the flow within the grenade is modeled excluding combustion of the pyrotechnic. Using chamber dimensions and payload chemical properties this simulation yields velocity, pressure, temperature, density and chemical compostion of the gas in the inner chamber and exiting the grenade.

2. NUMERICAL SIMULATION

The RAMCOMB (RAMjet COMBustion) computer code was originally developed for the numerical simulation of combustion in a tubular solid-fuel ramjet (SFRJ) projectile (Nusca et.al. 1988, Nusca 1989). Solid fuel regression rate and projectile thrust predictions compared favorably with in-flight and ground test data. For the SFRJ application the RAMCOMB code simulated a mass-controlled (stoichiometric) reaction of non-premixed solid fuel and oxygen using classical diffusion flame techniques. The code has also been used to simulate finite-rate premixed gaseous fuel combustion in the ram accelerator projectile launch system (Nusca 1991) with reaction rates formulated in terms of temperature and chemical species mass fraction. Application of the code to payload dissemination simulation for grenades involves chemical species ablation and diffusion without chemical reactions. The governing equations, boundary and initial conditions as well as the solution method are outlined below.

2.1 Governing Equations. Since the grenade payload chamber geometry is axisymmetric (Fig. 1) the governing equations can be written in cylindrical coordinates. The velocity components in this system are u,v, and w for the radial (r), azimuthal (θ), and axial (z) directions, respectively. Axisymmetric flow is assumed thus, all θ-derivatives are ignored; however, the azimuthal velocity component and the azimuthal momentum equation are retained (for future consideration of chamber rotation). Since steady flows are considered, time derivatives ($\partial/\partial t$) are ignored. The conservation equations for global mass, momentum (radial, axial, azimuthal) and species mass conservation are given by (Nusca 1991, Schlichting 1979),

$$\nabla \cdot \rho\vec{V} = \frac{1}{r}\frac{\partial(r\rho u)}{\partial r} + \frac{\partial(\rho w)}{\partial z} = 0 \tag{1}$$

$$\nabla \cdot [\rho u\vec{V} - \vec{\tau_r}] - \frac{1}{r}[\rho v^2 - \tau_{\theta\theta}] + \frac{\partial p}{\partial r} = 0 \tag{2}$$

$$\nabla \cdot [\rho w\vec{V} - \vec{\tau_z}] + \frac{\partial p}{\partial z} = 0 \tag{3}$$

$$\frac{1}{r}\nabla \cdot [r(\rho v\vec{V} - \vec{\tau_\theta})] = 0 \tag{4}$$

$$\frac{1}{r}\left[\frac{\partial}{\partial r}(r\rho u m_j + rJ_{j,r}) + \frac{\partial}{\partial z}(r\rho w m_j + rJ_{j,z})\right] = 0 \tag{5}$$

Energy conservation for a compressible flow is expressed by the First Law of Thermodynamics. The steady form of the First Law states that the net rate of stagnation enthalpy ($\tilde{h} = h + V^2/2$) inflow for a control volume is equal to the sum of the shear work done by the contents of the control volume on the surroundings ($\vec{\tau}$) and the heat transfer to the

surroundings (Schlichting 1979).

$$\nabla \cdot \left[\rho \vec{V} \tilde{h} + \vec{J}_h + \sum_{j=1}^{N} h_j \vec{J}_j + \vec{J}_k - (u \vec{\tau}_r + v \vec{\tau}_\theta + w \vec{\tau}_z) \right] = 0 \tag{6}$$

where $\vec{J}$ is a flux term for mass ($\vec{J}_j = (\mu_{\text{eff}}/\text{Re}) \nabla m_j = \Gamma_j \nabla m_j$), heat ($\vec{J}_h = (\mu_{\text{eff}}/\text{Pr}) c_{p_j} \nabla T = \Gamma_h c_{p_j} \nabla T$), and turbulence kinetic energy, k, ($\vec{J}_k = (\mu_{\text{eff}}/\text{Pr}) \nabla k = \Gamma_k \nabla k$). Where Γ represents the diffusion coefficient. The mass fraction and molar specific enthalpy for species j are m_j and h_j, respectively. The density, pressure, velocity vector and velocity magnitude are given by $\rho, p, \vec{V}, V = \sqrt{u^2 + v^2 + w^2}$, respectively.

In Equations 2-4,6 the shear stress ($\vec{\tau}$) includes the Reynolds stress with an effective fluid viscosity expressed as the sum of the molecular and turbulent viscosities, $\mu_{\text{eff}} = \mu + \mu_t$. The flow Reynolds number, Re, represents the ratio of mass flux ($\rho V L$) to fluid viscosity, μ_{eff}. Molecular viscosity (μ) is defined using Sutherland's expression (Ames 1958),

$$\mu = 2.270\text{x}10^{-8} \frac{T^{1.5}}{T + 198.6} \tag{7}$$

Turbulent viscosity (μ_t) is described in the next section of this report.

The calorically perfect gas assumption can be used to determine the specific heat of each species, c_{p_j}, when the temperature dependence of the species is not well determined. The specific heat can also be formulated using an explicit temperature dependence obtained from tabulated data (Stull and Prophet 1971).

$$c_{p_j}/\bar{\Re} = A_1 + A_2 T + A_3 T^2 + A_4 T^3 + A_5 T^4 \tag{8}$$

where the mixture specific heat is given by,

$$c_p = \sum_{j=1}^{N} m_j c_{p_j} \tag{9}$$

Mixture temperature (T) is obtained from the conservation of energy (Eq. 6) expressed in terms of the stagnation enthalpy,

$$\tilde{h} = T \sum_{j=1}^{N} c_{p_j} m_j + \left[1 - \frac{1}{\text{Pr}}\right] \frac{V^2}{2} + \left[\frac{1}{\text{Sc}} - \frac{1}{\text{Pr}}\right] \frac{\tilde{V}^2}{2} + \left[\frac{1}{\text{Sc}} - \frac{1}{\text{Pr}}\right] \sum_{j=1}^{N} h_j m_j \tag{10}$$

where $\tilde{V}$ is the magnitude of the turbulent (fluctuating) velocity, $\sqrt{k}$. The Schmidt number, $\text{Sc} = \mu_{\text{eff}}/(\rho \Gamma)$, (ratio of momentum transport to mass transport) is assumed to be unity. The Prandtl number, $\text{Pr} = c_p \mu_{\text{eff}}/\kappa$, (ratio of momentum transport to heat transport) is assumed to be nearly unity (.9) which is considered adequate for gaseous flows (Bradshaw 1981). The thermal conductivity of the gas mixture is denoted κ.

The mixture equation of state for a thermally perfect gas follows from Dalton's Law,

$$p = \rho\bar{\Re}T\sum_{j=1}^{N}\frac{m_j}{\mathcal{M}_j} \tag{11}$$

where $\bar{\Re} = \Re\sum_j \mathcal{M}_j$, $\mathcal{M}_j$ is the molecular weight of species j, and $\Re$ is the specific gas constant. Equation 11 is used to recover the density from the numerical solution of the governing equations.

The stream function-vorticity form of the governing equations has been widely utilized and facilitates the use of numerically efficient Gauss-Seidel relaxation algorithms. Stream function, ψ, and vorticity, ω are defined using (Schlichting 1979),

$$\frac{\partial\psi}{\partial r} = r\rho w, \qquad \frac{\partial\psi}{\partial z} = -r\rho u, \qquad \omega = \nabla\times\vec{V} = -\left[\frac{\partial}{\partial z}\left(\frac{1}{r\rho}\frac{\partial\psi}{\partial z}\right) + \frac{\partial}{\partial r}\left(\frac{1}{r\rho}\frac{\partial\psi}{\partial r}\right)\right] \tag{12}$$

The governing equations, derived by Nusca (1989), can be expressed in the form of a general variable, ϕ. This variable can represent stream-function, vorticity, azimuthal velocity, stagnation enthalpy, species mass fraction, turbulence kinetic energy, or turbulence dissipation rate.

$$a_\phi\left[\frac{\partial}{\partial z}\left(\phi\frac{\partial\psi}{\partial r}\right) - \frac{\partial}{\partial r}\left(\phi\frac{\partial\psi}{\partial z}\right)\right] - \frac{\partial}{\partial z}\left[b_\phi r\frac{\partial}{\partial z}(c_\phi\phi)\right] - \frac{\partial}{\partial r}\left[b_\phi r\frac{\partial}{\partial r}(c_\phi\phi)\right] + rd_\phi = 0 \tag{13}$$

For example, $\phi = \psi, a_\phi = 0, b_\phi = 1/(\rho r^2), c_\phi = 1, d_\phi = -\omega/r$ (which yields Eq. 12). For N species only $N-1$ specie equations ($\phi = m_j$) must be solved, since the sum of the mass fractions must equal unity. In effect the global continuity equation (Eq. 1) is the Nth specie equation since the summation of all specie equations yields the continuity equation.

The pressure can be recovered from the $\psi - \omega$ form of the equations after a converged solution of Equation 13 is achieved or after each iteration, if pressure variations are expected to have a significant effect on density. The radial and axial momentum equations (Eq. 2 and 3) can be rearranged to yield:

$$\frac{\partial p}{\partial z} = P_1(r,z) \quad\text{and}\quad \frac{\partial p}{\partial r} = P_2(r,z) \tag{14}$$

where P_1 and P_2 are functions of ρ, V and $\vec{r}$. Along any path from point A to point B in the flowfield, the pressure is given by:

$$p_B - p_A = \int_A^B (P_1 dz + P_2 dr) \tag{15}$$

Since p is a scalar, $p_B - p_A$ should be path independent and therefore, can serve as a consistency check on the converged solution. In most cases a pressure difference is desired to form the pressure coefficient at a point. However, if the pressure at point B is required the pressure at point A is assigned to a known inlet value and integration proceeds from the inlet to point B in the flowfield.

2.2 Turbulence Model. A two-equation turbulence model has been suggested by Kim and Chung (1989) for multiple species flows. This model describes the turbulence viscosity (μ_t) as a function of turbulence kinetic energy (k) and dissipation rate (ϵ) as $\mu_t = \rho C_3 k^2/\epsilon$. A set of partial differential equations is written for k and ϵ.

$$\rho w \frac{\partial k}{\partial z} + \rho u \frac{\partial k}{\partial r} - \frac{1}{r}\left[\frac{\partial}{\partial z}\left(r\mu_k \frac{\partial k}{\partial z}\right) + \frac{\partial}{\partial r}\left(r\mu_k \frac{\partial k}{\partial r}\right)\right] = G - \rho\epsilon \tag{16}$$

$$\rho w \frac{\partial \epsilon}{\partial z} + \rho u \frac{\partial \epsilon}{\partial r} - \frac{1}{r}\left[\frac{\partial}{\partial z}\left(r\mu_\epsilon \frac{\partial \epsilon}{\partial z}\right) + \frac{\partial}{\partial r}\left(r\mu_\epsilon \frac{\partial \epsilon}{\partial r}\right)\right] = \frac{C_1 G\epsilon}{k} - \frac{C_2\rho\epsilon^2}{k} \tag{17}$$

$$\frac{G}{\mu_t} = 2\left(\left(\frac{\partial w}{\partial z}\right)^2 + \left(\frac{\partial u}{\partial r}\right)^2 + \left(\frac{u}{r}\right)^2\right) + \left(\frac{\partial w}{\partial r} + \frac{\partial u}{\partial z}\right)^2 \tag{18}$$

where, $\mu_k = \mu + \mu_t/\lambda_k, \mu_\epsilon = \mu + \mu_t/\lambda_\epsilon, \lambda_k = 1, \lambda_\epsilon = 1.3, C_1 = 1.44, C_2 = 1.92, C_3 = .09$. These equations are solved along with the Navier-Stokes equations (Eq. 13) using,

$$\phi = k, a_\phi = 1, b_\phi = r\mu_k, c_\phi = 1, d_\phi = r(G - \rho\epsilon)$$

$$\phi = \epsilon, a_\phi = 1, b_\phi = r\mu_\epsilon, c_\phi = 1, d_\phi = r(C_1 G\epsilon/k - C_2\rho\epsilon^2/k)$$

2.3 Boundary and Initial Conditions. The boundaries of the inner grenade chamber (see Figure 1) are the inlet (connected to the pyrotechnic chamber), the exit (nozzle throat), the symmetry axis, the chamber wall lined with payload material, and a section of solid wall along the nozzle. Since the governing equations (Eq. 13) are elliptic the conditions along these boundaries must prescribe values of the dependent variables, the gradient of the dependent variables in the normal direction, or an algebraic relation which connects the values of the dependent variables to the normal component of velocity.

At the inlet plane, radial profiles of all dependent variables, $\psi, \omega, m_j, \tilde{h}, v, k,$ and ϵ as well as values for V, T, p, ρ, and μ_{eff} are specified. It is assumed that the flow at the inlet plane consists of air and that the diffusion of payload into the airstream from the chamber wall does not effect the inlet flow. During actual grenade operation the inlet flow consists of pyrotechnic combustion gases (e.g. H_2O, CO_2) the exact nature of which was unavailable for the numerical simulations. A subsonic inlet flow velocity assumption is used in accordance with the elliptic nature of the governing equations. Initial conditions for all dependent variables are supplied by the inlet boundary conditions. The turbulence model is initialized using $k = k_\infty = \alpha V_\infty^2, \epsilon = k^{1.5} C_3^{-0.5}/(.37x^{0.8}\mathrm{Re}^{-0.4})$. The initial turbulence kinetic energy is specified as $(1/\alpha)\%$ of the inlet kinetic energy.

The exit plane is located at the nozzle throat where the flow is assumed to be subsonic. The streamlines at the exit plane are assumed to be parallel to the symmetry axis; thus, the gradients of all dependent variables along these streamlines are zero. These assumptions are

reasonable since experience for large Reynolds numbers has shown that the exact nature of the exit plane boundary conditions has little effect on the flowfield solution when convection is significant (i.e. large inlet mass flow) (Bradshaw et.al. 1981, Khalil et.al. 1975).

For mass continuity, the symmetry axis is considered to be a streamline of the flow, thus ψ = constant. Along the symmetry axis $r = 0$, thus $\partial\psi/\partial z = \partial\psi/\partial r = 0$ via Equation 12. The value of ψ along this boundary can be determined from values of ψ adjacent to the boundary using a one-sided finite-difference for $\partial\psi/\partial r$ at the axis. From Equation 12, the boundary value for ω is zero. The axis boundary values for the remaining dependent variables, ϕ, are determined from $\partial\phi/\partial r = 0$.

The no-slip condition ($u = w = 0$, and $v/r = \Omega$, where Ω is the wall spinrate) is applied to the solid walls. Therefore ψ = constant, via Equation 12. For convenience $\psi = 0$ is chosen. One-sided finite-differences for $\partial\psi/\partial r$ and $\partial\psi/\partial z$ are used in Equation 12 to determine the wall value for ω. For an inert wall, the normal gradient of all mass fractions, $\partial m_j/\partial \mathrm{n}$, are set to zero. For a wall with payload material, the boundary condition is based on the assumption that the payload material is continually vaporizing ($m_{\mathrm{payload}} = 1, m_{\mathrm{air}} = 0, m_{\mathrm{mixture}} = 0$). The wall temperature is set to the vaporization temperature of the payload, $T_{\mathrm{wall}} = T_{\mathrm{vap}}$. Figure 2 shows the results of a thermogravimetric analysis of yellow dye (i.e. payload material) (Turetsky 1991). The percent weight loss of the sample is plotted as a function of temperature. Note that vaporization of the material (i.e. significant weight loss) occurs over a narrow temperature range, supporting the use of such a boundary condition. The rate of burning (regression rate) on the payload surface varies as a function of position along the surface and is computed from the temperature gradient normal to the wall,

$$\dot{r} = \frac{-\kappa_{\mathrm{p}}}{\rho_{\mathrm{p}} h_{\mathrm{vap}}} \frac{\partial T}{\partial r} \tag{19}$$

where κ_{p} and ρ_{p} are the thermal conductivity and density of the solid payload, and h_{vap} is the heat of vaporization of a unit mass of payload. Values of the thermal conductivity, density, and heat of vaporization can be determined for most grenade payload materials.

The boundary conditions for the payload surface are based on the assumption of single diffusion, i.e. diffusion of gaseous payload molecules into the airstream without diffusion of air molecules into the payload material. Single diffusion has been studied by R.D. Present (1958). The general equation of mutual/thermal diffusion is given by,

$$G_j = n_j u_j - n\Gamma \frac{d}{dz}\left(\frac{n_j}{n}\right) + \frac{n_j \Gamma_T}{T}\frac{dT}{dz} \qquad (j = 1,2) \tag{20}$$

where n_j = molecular density of species j, $n = \sum_j n_j$, u_j = convection velocity of species j, z = diffusion direction, Γ = mass diffusion coefficient ($V\lambda/3$, λ = the molecular mean free path), and Γ_T = thermal diffusion coefficient ($\kappa/(\rho h_{\mathrm{vap}})$). The equation of "single diffusion"

can be obtained by assuming that air molecules (j=1) are moving in a boundary layer so that $u_1 \simeq 0$ and payload molecules (j=2) are at rest, $u_2 \equiv 0$. In addition, the payload molecules are closely packed so that $n_1 \ll n_2$. As a result,

$$G_{\text{air}} = G_1 \simeq 0, \qquad G_{\text{payload}} = G_2 \simeq -(n_1+n_2)\Gamma\frac{d}{dz}\left(\frac{n_2}{n_1+n_2}\right) + \frac{n_2\Gamma_T}{T}\frac{dT}{dz} \tag{21}$$

The mass diffusion terms of Equation 21 are incorporated in the J_j terms of Equation 5 and Γ_T is customarily neglected.

The payload surface boundary condition may also be prescribed using a surface ablation model such as described by Moss (1976). In this model the payload vaporization temperature and heat of vaporization are prescribed as functions of the pressure applied to the material surface. An equation similar to Equation 19 is used along with these functions in a iterative/coupling procedure with the governing equations in order to prescribe the payload surface boundary condition. The use of an ablation model, as opposed to assuming that the payload surface is continually vaporizing ($T_{\text{wall}} = T_{\text{vap}}$) is more critical for cases where the vaporization characteristics of the material are a strong function of pressure and temperature (i.e. unlike that shown in Fig. 2). The major drawback to using an ablation model is the increased computational cost of the iterative procedure and the requirement of experimental data in the form $T_{\text{vap}} = T_{\text{vap}}(p), h_{\text{vap}} = h_{\text{vap}}(p)$.

Boundary conditions for turbulence variables, k and ϵ, are $k = 0, \epsilon = .056\mu(\partial u/\partial r)^2/\rho$ for solid walls and $k = 10^{-6}V_\infty^2, \epsilon = k^{1.5}/L$ for the inlet flow. Along the chamber axis and exit plane $\partial k/\partial r = \partial\epsilon/\partial r = 0, \partial k/\partial z = \partial\epsilon/\partial z = 0$, respectively.

2.4 Computational Algorithm. Equation 13 can be reduced to a successive-substitution formula for flow variable ϕ at each node on the computational grid. Central finite-differences are used for the diffusive and source terms and upwind differences for the convective terms. Using upwind differencing in the species conservation equations (Eq. 5) reduces the occurrence of negative species mass fractions in mixing layers. The resulting system of equations for the entire grid is solved using a Gauss-Seidel relaxation scheme (Nusca 1989). Each iteration cycle is made up of M sub-cycles, where M is the number of equations being considered (M must be at least 2 since the equations for $\phi = \omega/r$ and $\phi = \psi$ are the minimum required to define the flow). In each sub-cycle, grid points are scanned row by row and a single variable is updated. The variables ω/r and ψ are updated in order followed by all other variables. When all sub-cycles are completed a new iteration cycle is started in which the values of the variables from the latest iteration are immediately used. This is consistent with the Gauss-Seidel methodology (Carnahan 1969). Convergence is satisfied when the greatest relative change in any flow variable is smaller than a prescribed tolerance.

3. RESULTS

In order to demonstrate the numerical method, simulations were performed for an experimental grenade model loaded with yellow dye payload simulant that has been the subject of testing at CRDEC. In these tests the grenade's inner chamber was instrumented with pressure transducers and thermocouples (for temperature measurements). The chamber was lined with yellow dye payload material about .25 inches in thickness. A typical test run yields measured values for the chamber inlet pressure and temperature (due mainly to pyrotechnic ignition) of about 3.5 psig (1.24 atm) and 425 C. The nozzle or exit plane values were measured as 1.5 psig (1.1 atm) and 375 C. These values were used as boundary conditions for the numerical simulation. The chemical properties of the yellow dye payload material were measured as $T_{\text{vap}} = 241$ C, $h_{\text{vap}} = 102.9$ J/g, $\mathcal{M} = 273$ g/mole. The density and thermal conductivity of the dye have not been measured but were taken as $\rho_{\text{p}} = 1.8$ g/mole and $\kappa_{\text{p}} = .00143$ cal/s-cm-C, respectively. Sensitivity studies using the present numerical model show that the predicted payload regression rate depends significantly on the value of κ_{p} and less on the value of ρ_{p}. The inlet gas was assumed to be air with $\mathcal{M} = 28.8$ g/mole and the $\mathcal{M}$ of the air/payload gas mixture taken as 150 g/mole.

Figure 3 shows the computational grid (or mesh) used for flowfield simulation within the grenade's inner chamber, bounded axially by the inlet and nozzle and radially by the symmetry axis and chamber wall. The chamber is cylindrical with an overall length of 4.0 inches and .375 inches in diameter. These dimensions represent the chamber shape before payload surface regression. Note that the vertical axis in Figure 3 has been magnified for clarity by a factor of 10 over the horizontal axis. About 131 grid points were used in the axial direction with 35 points in the radial direction; the grid points were unevenly distributed in order to cluster points along the boundaries (except at the symmetry axis). Figure 4 shows the computed velocity vectors (i.e. arrows whose length is representative of the magnitude of local gas velocity and direction indicates the orientation of the local velocity) displayed at every 6th axial grid point and every other radial point (for clarity). A thick boundary layer that develops along the chamber wall (i.e. payload surface) can be observed. The computed average chamber exit velocity is approximately 121 ft/s. The surface of the payload material was allowed to ablate (i.e. regress) for .25 seconds resulting in the shape shown in Figure 5 (computational grid). Note that the material surface has been blunted at the chamber inlet but more evenly eroded over most of the surface with the exception of a discontinuity at the payload/nozzle wall junction ($z = 3.5$ inches). Figure 6 shows the computed velocity vectors for this chamber shape. Due to the contour of the chamber entrance, the flow is significantly accelerated (indicated by longer arrows in the figure) forming a thinner boundary layer along the payload surface (i.e. larger Re). The computed average chamber exit velocity is

approximately 276 ft/s. Figure 7 shows the distribution of payload regression rate (Eq. 19) along the payload surface for both the initial time and .25 seconds elapsed time. Payload regression rate is largest near the chamber inlet and nearly uniform over most of the payload surface. The regression rate increases with elapsed time.

Figure 8 shows radial profiles of axial velocity component at both the initial and elapsed time as well as two axial positions along the chamber - midlength, $z = 2$in, and the exit plane, $z = 4$in. Consistent with the imposed boundary conditions the velocity is zero at the chamber wall ($r = .1875$in) and the velocity gradient is zero at the chamber axis ($r = 0$). The retarding effect of the wall boundary layer on the velocity profile can also be observed. Note that the profiles at chamber midlength show the payload surface regressing from $r =$ .1875in to about .195in from the centerline while the profiles at chamber exit show no wall regression since the chamber wall is solid at this location. Comparing the chamber midlength profiles with those at the exit plane show that the boundary layer (or mixing layer) thickens with axial location downstream of the inlet. Comparing the initial time profiles with those at the elapsed time show that the gas flow is significantly accelerated as the payload surface regresses and the boundary layer thickness decreases (i.e. larger Re).

Figure 9 shows radial profiles of gas temperature at both the initial and elapsed time as well as two axial positions along the chamber - midlength, $z = 2$in, and the exit plane, $z = 4$in. Consistent with the imposed boundary conditions the temperature is T_{vap} at the payload surface while the temperature gradient is zero at both the chamber axis and the solid chamber wall at the nozzle (adiabatic wall condition). Note that the profiles at chamber midlength show the payload surface regressing from r = .1875in to about .195in from the centerline while the profiles at chamber exit show no wall regression since the chamber wall is solid at this location. Within the boundary layer established on the payload surface the temperature of the air/payload mixture is gradually increased until it reaches the centerline (i.e. inlet) value. Comparing the chamber midlength profiles with those at the exit plane show that the thermal boundary layer thickens with axial location downstream of the inlet. Comparing the initial time profiles with those at the elapsed time show that the gas flow is slightly hotter at any chosen radial position within the mixing layer.

Figures 10 and 11 show radial profiles of mixture (payload + air) mass fraction at both the initial and elapsed time as well as two axial positions along the chamber - midlength, $z = 2$in, and the exit plane, $z = 4$in. Consistent with the imposed boundary conditions the mixture mass fraction, m_{mixture}, is zero at the payload surface (i.e. $m_{\text{payload}} = 1$, $m_{\text{air}} = 0$) and along the chamber centerline (i.e. $m_{\text{payload}} = 0$, $m_{\text{air}} = 1$). Along solid walls (i.e. chamber exit) and at the chamber centerline the gradient of m_{mixture} is zero. The mixture mass fraction is exactly or nearly unity at some point in the flowfield where m_{payload} and

m_{air} are equivalent. Note that the profiles at chamber midlength show the payload surface regressing from r = .1875in to about .195in from the centerline while the profiles at chamber exit show no wall regression since the chamber wall is solid at this location. Comparing the chamber midlength profiles with those at the exit plane show that the chamber core flow, consisting of air ($m_{mixture} = 0$), thins from a radial position of about .12in to .10in at the initial time and .15in to .13in at the elapsed time. The diffusion of payload material into the core flow is advanced with axial position as the boundary layer imposed on the payload surface grows. Comparing the initial time profiles with those at the elapsed time show that the mixing layer (i.e. highest mixture concentration) follows the payload surface as regression progresses.

4. CONCLUSIONS

Material dissemination from the payload chamber inside a dual-chamber grenade has been simulated using computational fluid dynamics. A thermal dissemination technique that uses the hot, moving gases generated from combustion of a pyrotechnic within the grenade has been investigated. The dissemination process is initiated by ablation and vaporization of the payload material from exposure to the thermal effects of pyrotechnic combustion. This material in gaseous form is entrained in this flow and expelled from the grenade. The Navier-Stokes equations along with chemical species conservation equations were used to simulate the diffusion and convection processes of the flowfield within the grenade's payload chamber. Numerical simulations reveal that diffusion of the payload material is accomplished within a boundary layer that is established along the payload surface (chamber wall) and that a core flow, basically unaffected by the payload ablation, resides over about one-half of the chamber diameter. Thermal exposure of the payload mixture to the hot combustion gases from the pyrotechnic is concentrated in this layer where the temperature is below that of the core flow gases. As the payload surface regresses, the flow thru the chamber is accelerated and the diffusion/mixing layer follows the regressing surface which results in an expansion of the core flow. The regression rate increases with elapsed time (since pyrotechnic ignition) as the shape of the payload surface (chamber wall) is contoured by material ablation.

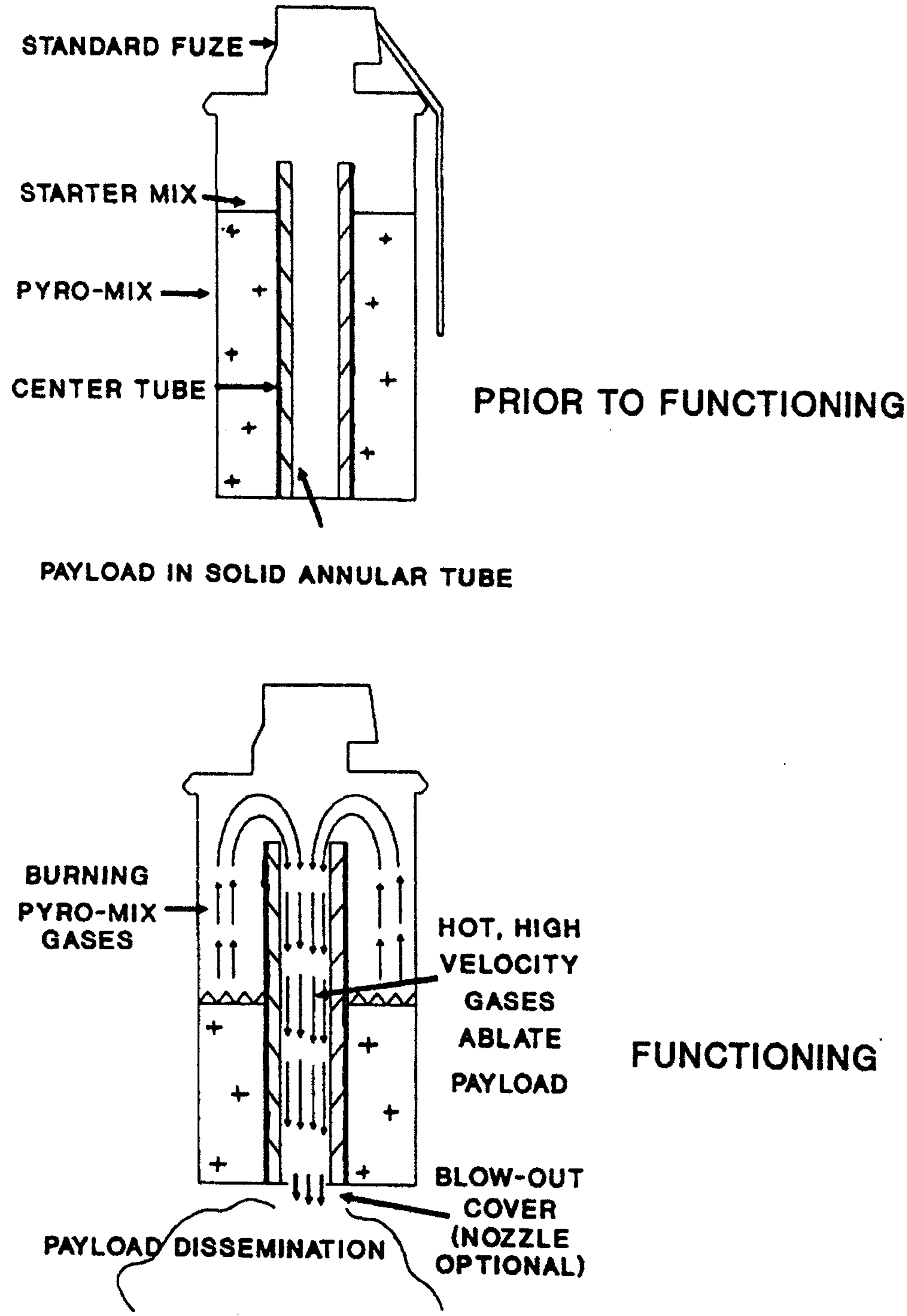

Figure 1. Schematic showing operation of the dual-chamber grenade thermal dissemination (M. Miller, U.S. Army CRDEC, used with permission)

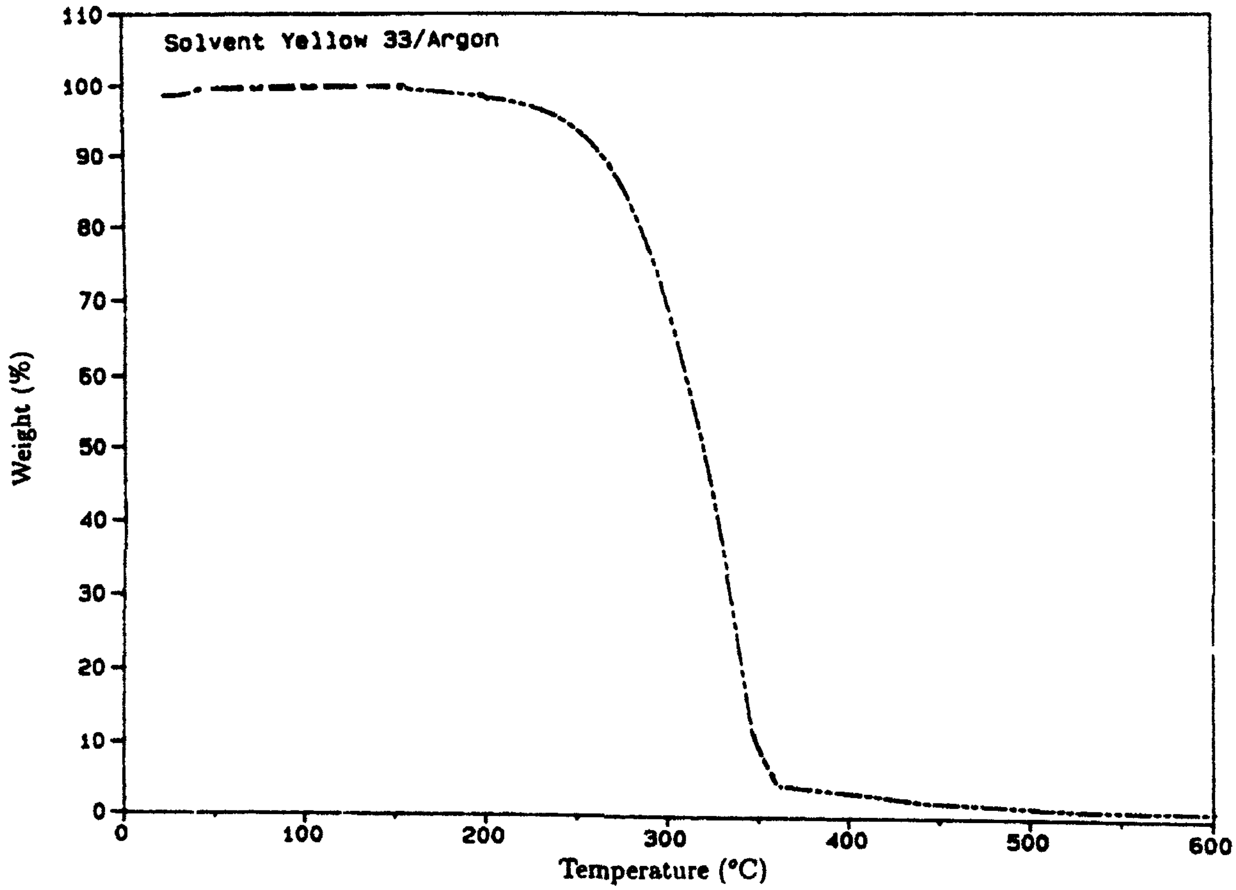

Figure 2. Measured weight change (%) of solvent yellow dye sample during heating from 0 to 600 C in argon atmosphere. Measurements done using thermogravimetric analyzer at CRDEC (Turetsky 1991)

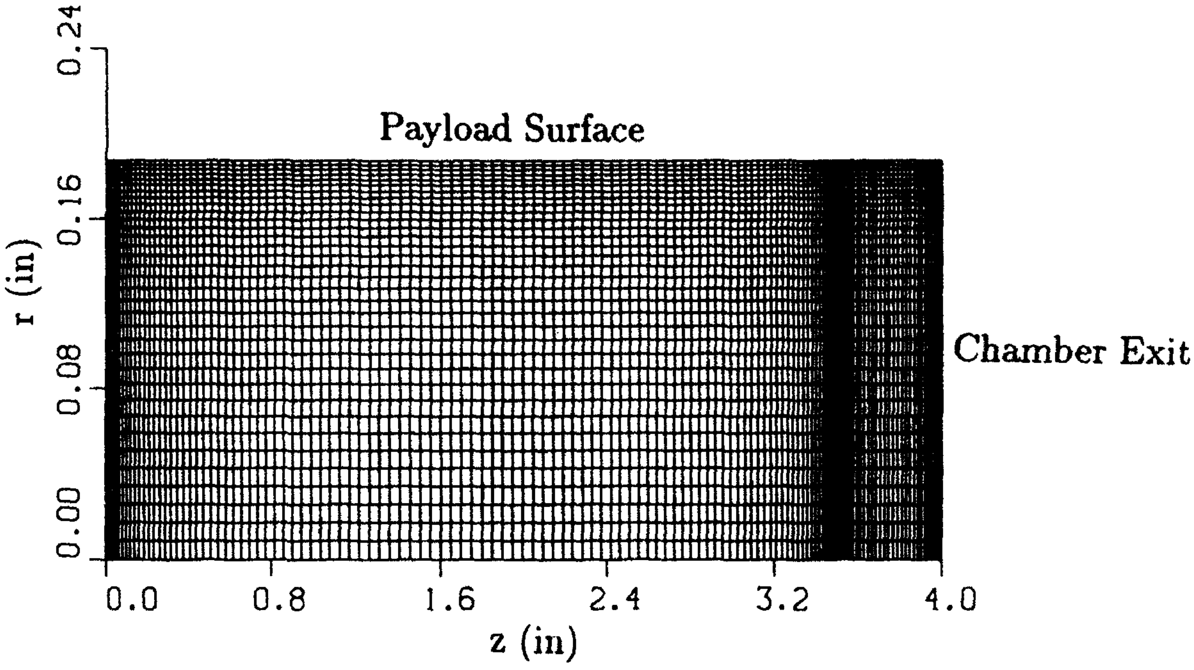

Figure 3. Computational grid for initial chamber shape

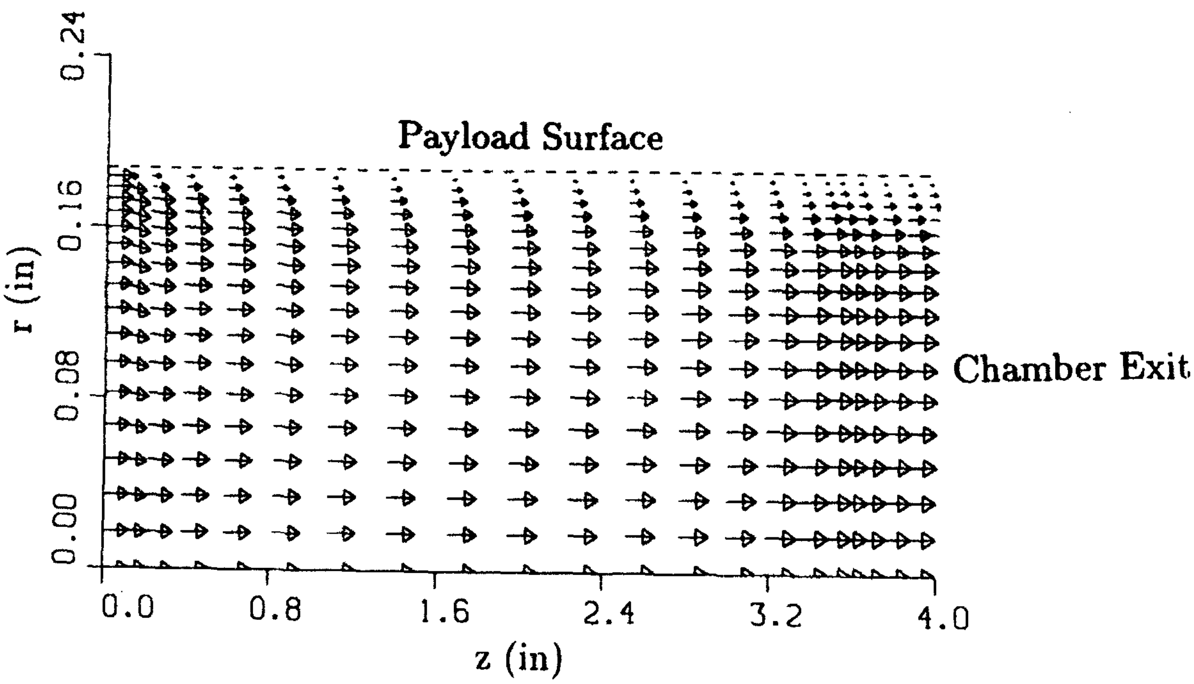

Figure 4. Computed velocity vector field for initial chamber shape

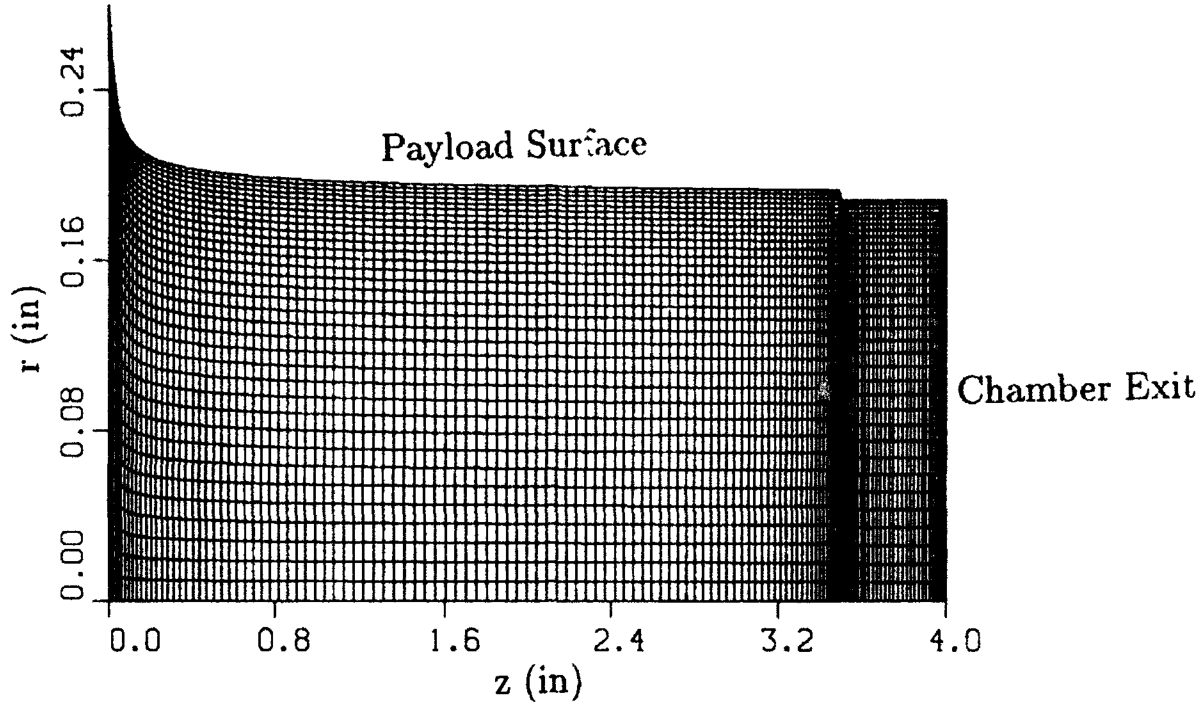

Figure 5. Computational grid for chamber shape after .25 seconds of payload surface ablation

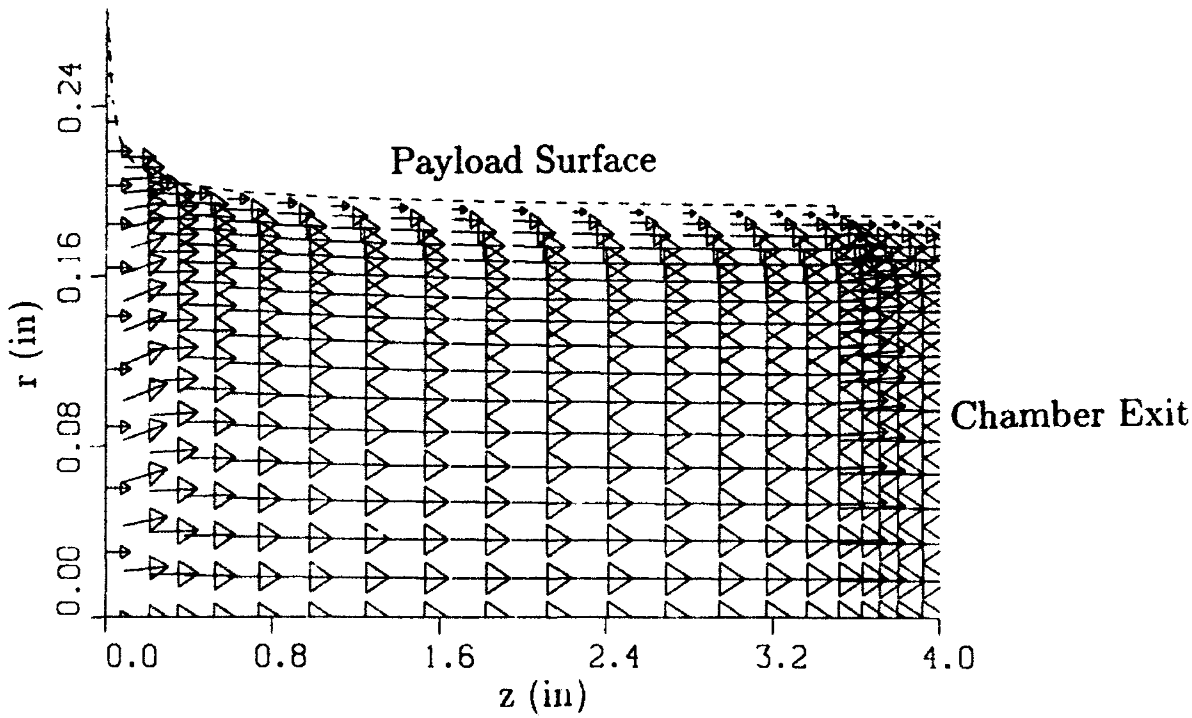

Figure 6. Computed velocity vector field for chamber shape after .25 seconds of payload surface ablation

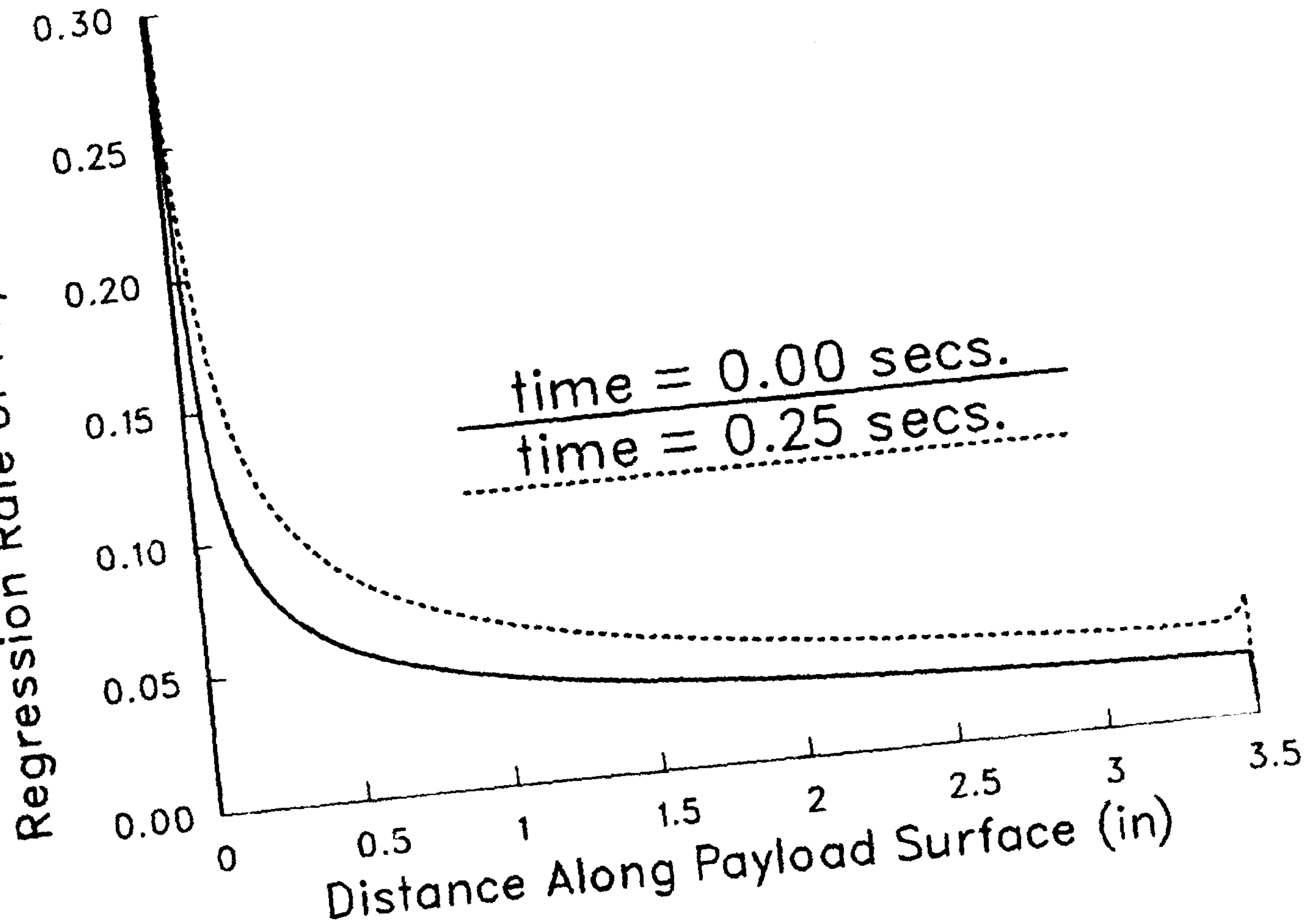

Figure 7. Computed payload material regression rate as a function of distance along payload surface, results for initial and elapsed time shown

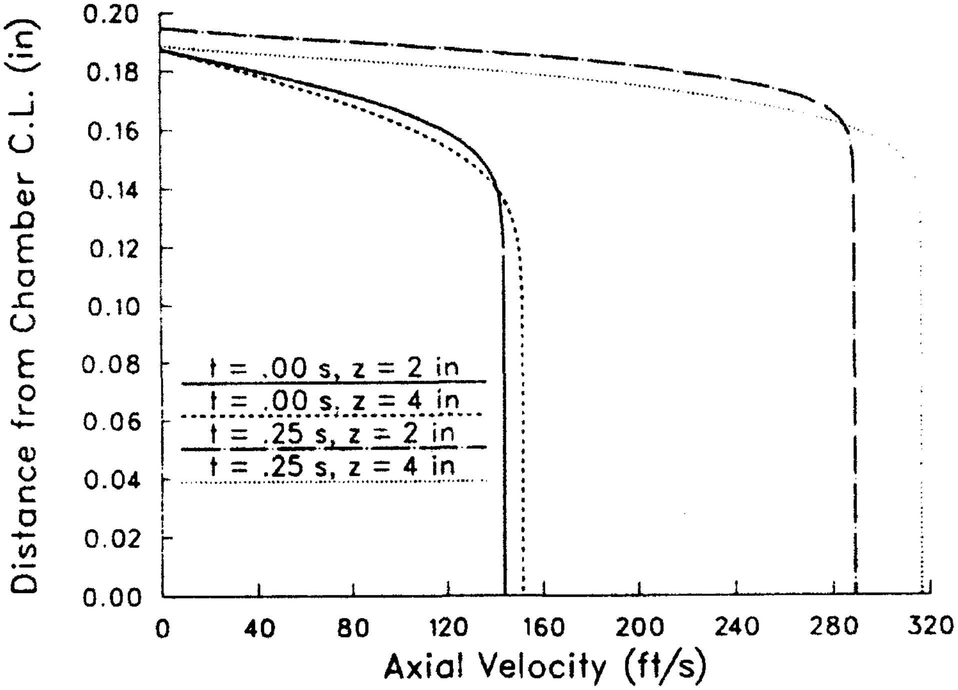

Figure 8. Computed radial profiles of axial component of gas flow velocity; results for initial and elapsed time shown at the chamber midlength and nozzle exit

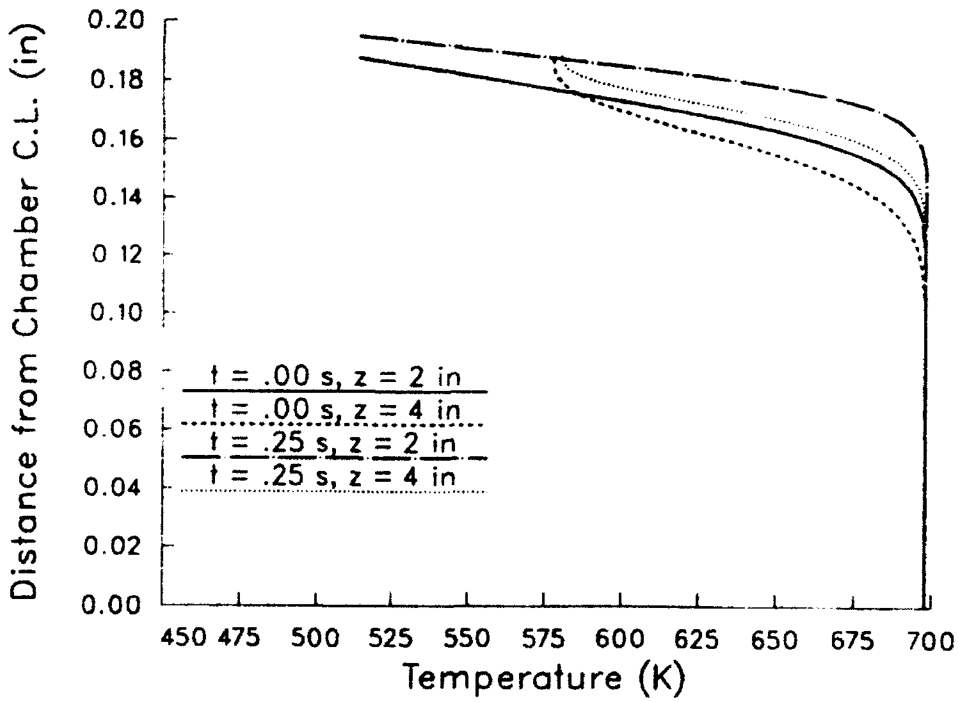

Figure 9. Computed radial profiles of gas temperature; results for initial and elapsed time shown at the chamber midlength and nozzle exit

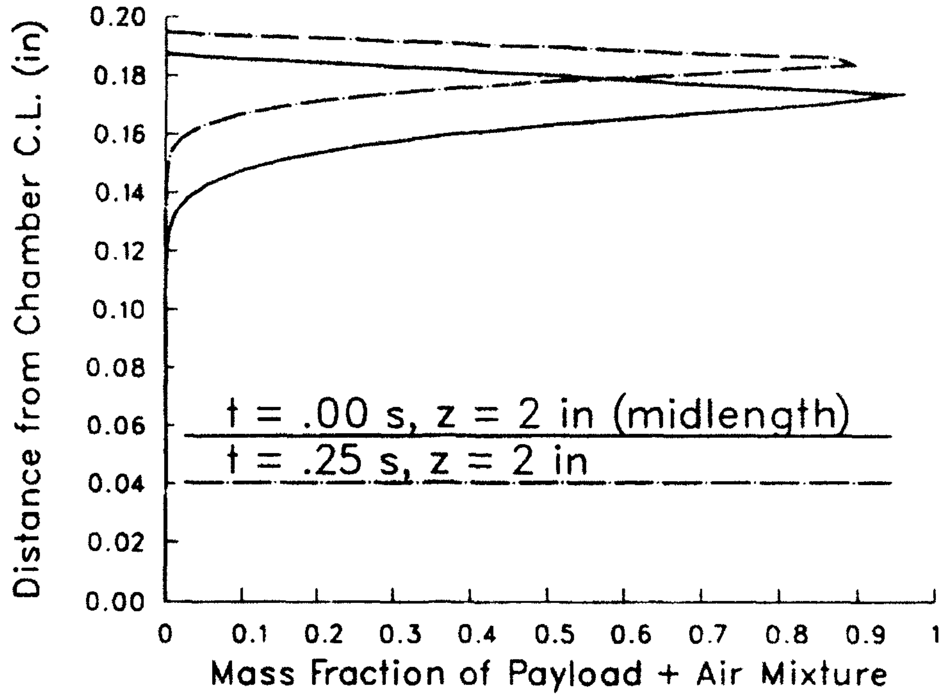

Figure 10. Computed radial profiles of gas composition (mixture mass fraction); results for initial and elapsed time shown at the chamber midlength

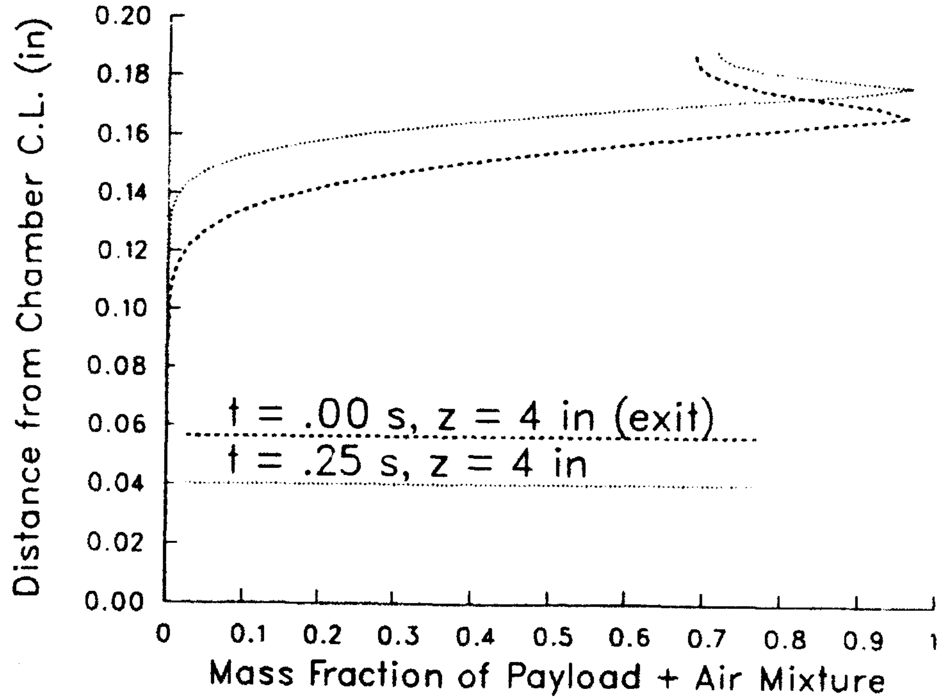

Figure 11. Computed radial profiles of gas composition (mixture mass fraction); results for initial and elapsed time shown at the chamber nozzle exit

INTENTIONALLY LEFT BLANK

5. REFERENCES

Ames Research Staff, "Equations, Tables, and Charts for Compressible Flow," NACA Report 1135, 1958.

Bradshaw, P., Cebeci, T., and Whitelaw, J.H., Engineering Calculation Methods for Turbulent Flows, Academic Press, New York, 1981.

Carnahan, B., Luther, H.A., and Wilkes, J.O., Applied Numerical Methods, John Wiley and Sons, New York, 1969.

Khalil, E.E., Spalding, D.B., and Whitelaw, J.H., "The Calculation of Local Flow Properties in Two-Dimensional Furnaces," International Journal of Heat and Mass Transfer, 1975, Vol. 18, pp. 775.

Kim, Y.M., and Chung, T.J., "Finite-Element Analysis of Turbulent Diffusion Flames," AIAA Journal, Vol. 27, No. 3, March 1989, pp. 330-339.

Moss, J.N., "Radiative Viscous-Shock-Layer Solutions with Coupled Ablation Injection," AIAA Journal, Vol. 14, No. 9, Sept. 1976, pp. 1311-1317.

Nusca, M.J., Chakravarthy, S.R., Goldberg, U.C., "Computational Fluid Dynamics Capability for the Solid-Fuel Ramjet Projectile," BRL-TR-2958, U.S. Army Ballistic Research Laboratory, Aberdeen Proving Ground, MD, December, 1988. (See also, AIAA Journal of Propulsion and Power, Vol. 6, No. 3, May-June 1990, pp. 256-262.)

Nusca, M.J., "Steady Flow Combustion Model for Solid-Fuel Ramjet Projectiles," BRL-TR-2987, U.S. Army Ballistic Research Laboratory, Aberdeen Proving Ground, MD, April, 1989. (See also, AIAA Journal of Propulsion and Power, Vol. 6, No. 3, May-June 1990, pp. 348-352.)

Nusca, M.J., "Numerical Simulation of Reacting Flow in a Thermally Choked Ram Accelerator - Model Development and Validation," BRL-TR-3222, U.S. Army Ballistic Research

Laboratory, Aberdeen Proving Ground, MD, April, 1991. (See also, AIAA-91-2490, Proceedings of the 27th AIAA Joint Propulsion Conference, June 24-27, 1991, Sacramento, CA, and Proceedings of the 28th JANNAF Combustion Subcommittee Meeting, Brooks AFB, San Antonio, TX, Oct. 28 - Nov. 1, 1991.)

Present, R.D., Kinetic Theory of Gases, McGraw-Hill Book Co., New York, 1958.

Schlichting, H., Boundary Layer Theory, 7th ed., translated by J. Kestin, McGraw-Hill, NY, 1979.

Stull, D.R., and Prophet, H., "JANNAF Thermochemical Tables," 2nd ed., National Bureau of Standards, NSRDS-Rept. 37, June 1971.

Turetsky, A., personal communication, U.S. Army Chemical Research Development and Engineering Center (CRDEC), Aberdeen Proving Ground, MD, December 1991.

LIST OF SYMBOLS

c_p	specific heat capacity, constant p
h	molar specific enthalpy
$\tilde{h}$	total enthalpy
h_{vap}	payload material heat of vaporization
J	flow rate or flux
k	turbulence kinetic energy
L	characteristic length
m	species mass fraction
$\mathcal{M}$	molecular weight
n	molecular density
N	number of species
p	static pressure
Pr	Prandtl Number
r	radial direction
$\dot{r}$	payload surface regression rate
$\Re$	specific gas constant, $(\gamma - 1)c_p/\gamma$
$\bar{\Re}$	universal gas constant, $\Re \sum_j \mathcal{M}_j$
Re	Reynolds Number
Sc	Schmidt Number
t	time
T	static temperature
u	radial velocity component
v	azimuthal velocity component
V	magnitude of the local velocity vector
$\vec{V}$	$u\hat{r} + v\hat{\theta} + w\hat{z}$
w	axial velocity component
X	mole fraction
z	axial direction

Greek Symbols

γ	ratio of specific heats
Γ	diffusion coefficient
ϵ	turbulence dissipation rate
θ	azimuthal direction
κ	thermal conductivity
μ	molecular viscosity
ρ	density
$\vec{\tau}$	shear stress vector
ϕ	general flow variable
ψ	stream function
ω	vorticity

Superscripts

$\hat{}$	unit vector
$\tilde{}$	total or stagnation quantity
$\dot{}$	rate

Subscripts

eff	effective
h	enthalpy contribution
j	j-th mixture component or species
k	turbulence kinetic energy contribution
p	constant pressure
p	payload quantity
r	radial component or radial direction
t	turbulence quantity

z	axial component
ϵ	turbulence dissipation rate
θ	azimuthal component
∞	freestream quantity

INTENTIONALLY LEFT BLANK

No. of Copies	Organization
2	Administrator Defense Technical Info Center ATTN: DTIC-DDA Cameron Station Alexandria, VA 22304-6145
1	Commander U.S. Army Materiel Command ATTN: AMCAM 5001 Eisenhower Ave. Alexandria, VA 22333-0001
1	Director U.S. Army Research Laboratory ATTN: AMSRL-D 2800 Powder Mill Rd. Adelphi, MD 20783-1145
1	Director U.S. Army Research Laboratory ATTN: AMSRL-OP-CI-AD, Tech Publishing 2800 Powder Mill Rd. Adelphi, MD 20783-1145
2	Commander U.S. Army Armament Research, Development, and Engineering Center ATTN: SMCAR-IMI-I Picatinny Arsenal, NJ 07806-5000
2	Commander U.S. Army Armament Research, Development, and Engineering Center ATTN: SMCAR-TDC Picatinny Arsenal, NJ 07806-5000
1	Director Benet Weapons Laboratory U.S. Army Armament Research, Development, and Engineering Center ATTN: SMCAR-CCB-TL Watervliet, NY 12189-4050
(Unclass. only)1	Commander U.S. Army Rock Island Arsenal ATTN: SMCRI-IMC-RT/Technical Library Rock Island, IL 61299-5000
1	Director U.S. Army Aviation Research and Technology Activity ATTN: SAVRT-R (Library) M/S 219-3 Ames Research Center Moffett Field, CA 94035-1000

No. of Copies	Organization
1	Commander U.S. Army Missile Command ATTN: AMSMI-RD-CS-R (DOC) Redstone Arsenal, AL 35898-5010
1	Commander U.S. Army Tank-Automotive Command ATTN: ASQNC-TAC-DIT (Technical Information Center) Warren, MI 48397-5000
1	Director U.S. Army TRADOC Analysis Command ATTN: ATRC-WSR White Sands Missile Range, NM 88002-5502
1	Commandant U.S. Army Field Artillery School ATTN: ATSF-CSI Ft. Sill, OK 73503-5000
(Class. only)1	Commandant U.S. Army Infantry School ATTN: ATSH-CD (Security Mgr.) Fort Benning, GA 31905-5660
(Unclass. only)1	Commandant U.S. Army Infantry School ATTN: ATSH-CD-CSO-OR Fort Benning, GA 31905-5660
1	WL/MNOI Eglin AFB, FL 32542-5000
	Aberdeen Proving Ground
2	Dir, USAMSAA ATTN: AMXSY-D AMXSY-MP, H. Cohen
1	Cdr, USATECOM ATTN: AMSTE-TC
1	Dir, ERDEC ATTN: SCBRD-RT
1	Cdr, CBDA ATTN: AMSCB-CI
1	Dir, USARL ATTN: AMSRL-SL-I
10	Dir, USARL ATTN: AMSRL-OP-CI-B (Tech Lib)

No. of Copies	Organization
1	Chairman DOD Explosives Safety Board Room 856-C Hoffman Bldg. 1 2461 Eisenhower Avenue Alexandria, VA 22331-0600
1	Headquarters U.S. Army Materiel Command ATTN: AMCICP-AD, M. Fisette 5001 Eisenhower Ave. Alexandria, VA 22333-0001
1	U.S. Army Ballistic Missile Defense Systems Command Advanced Technology Center P.O. Box 1500 Huntsville, AL 35807-3801
1	Department of the Army Office of the Product Manager 155mm Howitzer, M109A6, Paladin ATTN: SFAE-AR-HIP-IP, Mr. R. De Kleine Picatinny Arsenal, NJ 07806-5000
3	Project Manager Advanced Field Artillery System ATTN: SFAE-ASM-AF-E LTC D. Ellis T. Kuriata J. Shields Picatinny Arsenal, NJ 07801-5000
1	Project Manager Advanced Field Artillery System ATTN: SFAE-ASM-AF-Q, W. Warren Picatinny Arsenal, NJ 07801-5000
2	Commander Production Base Modernization Agency U.S. Army Armament Research, Development, and Engineering Center ATTN: AMSMC-PBM, A. Siklosi AMSMC-PBM-E, L. Laibson Picatinny Arsenal, NJ 07806-5000
4	PEO-Armaments Project Manager Tank Main Armament System ATTN: AMCPM-TMA AMCPM-TMA-105 AMCPM-TMA-120 AMCPM-TMA-AS, H. Yuen Picatinny Arsenal, NJ 07806-5000
5	Commander U.S. Army Armament Research, Development, and Engineering Center ATTN: SMCAR-CCD, D. Spring SMCAR-CCH-V, C. Mandala E. Fennell SMCAR-CCH-T, L. Rosendorf SMCAR-CCS Picatinny Arsenal, NJ 07806-5000
19	Commander U.S. Army Armament Research, Development, and Engineering Center ATTN: SMCAR-AEE, J. Lannon SMCAR-AEE-B, A. Beardell D. Downs S. Einstein S. Westley S. Bernstein J. Rutkowski B. Brodman P. O'Reilly R. Cirincione A. Grabowsky P. Hui J. O'Reilly SMCAR-AEE-WW, M. Mezger J. Pinto D. Wiegand P. Lu C. Hu SMCAR-AES, S. Kaplowitz Picatinny Arsenal, NJ 07806-5000
1	Commander U.S. Army Armament Research, Development and Engineering Center ATTN: SMCAR-HFM, E. Barrieres Picatinny Arsenal, NJ 07806-5000

No. of Copies	Organization
9	Commander U.S. Army Armament Research, Development and Engineering Center ATTN: SMCAR-FSA-T, M. Salsbury SMCAR-FSA-F, LTC R. Riddle SMCAR-FSC, G. Ferdinand SMCAR-FS, T. Gora SMCAR-FS-DH, J. Feneck SMCAR-FSS-A, R. Kopman B. Machek L. Pinder SMCAR-FSN-N, K. Chung Picatinny Arsenal, NJ 07806-5000
3	Director Benet Weapons Laboratories ATTN: SMCAR-CCB-RA, G.P. O'Hara G.A. Pflegl SMCAR-CCB-S, F. Heiser Watervliet, NY 12189-4050
2	Commander U.S. Army Research Office ATTN: Technical Library D. Mann P.O. Box 12211 Research Triangle Park, NC 27709-2211
1	Commander, USACECOM R&D Technical Library ATTN: ASQNC-ELC-IS-L-R, Myer Center Fort Monmouth, NJ 07703-5301
1	Commander U.S. Army Harry Diamond Laboratory ATTN: SLCHD-TA-L 2800 Powder Mill Rd. Adelphi, MD 20783-1145
1	Commandant U.S. Army Aviation School ATTN: Aviation Agency Fort Rucker, AL 36360
1	Program Manager U.S. Tank-Automotive Command ATTN: AMCPM-ABMS, T. Dean Warren, MI 48092-2498

No. of Copies	Organization
1	Project Manager U.S. Tank-Automotive Command Fighting Vehicle Systems ATTN: SFAE-ASM-BV Warren, MI 48397-5000
1	Project Manager, Abrams Tank System ATTN: SFAE-ASM-AB Warren, MI 48397-5000
1	Director HQ, TRAC RPD ATTN: ATCD-MA Fort Monroe, VA 23651-5143
2	Director U.S. Army Materials Technology Laboratory ATTN: SLCMT-ATL (2 cps) Watertown, MA 02172-0001
1	Commander U.S. Army Belvoir Research and Development Center ATTN: STRBE-WC Fort Belvoir, VA 22060-5006
1	Director U.S. Army TRAC-Ft. Lee ATTN: ATRC-L, Mr. Cameron Fort Lee, VA 23801-6140
1	Commandant U.S. Army Command and General Staff College Fort Leavenworth, KS 66027
1	Commandant U.S. Army Special Warfare School ATTN: Rev and Trng Lit Div Fort Bragg, NC 28307
1	Commander Radford Army Ammunition Plant ATTN: SMCAR-QA/HI LIB Radford, VA 24141-0298

No. of Copies	Organization
1	Commander U.S. Army Foreign Science and Technology Center ATTN: AMXST-MC-3 220 Seventh Street, NE Charlottesville, VA 22901-5396
2	Commandant U.S. Army Field Artillery Center and School ATTN: ATSF-CO-MW, E. Dublisky ATSF-CN, P. Gross Ft. Sill, OK 73503-5600
1	Commandant U.S. Army Armor School ATTN: ATZK-CD-MS, M. Falkovitch Armor Agency Fort Knox, KY 40121-5215
2	Commander Naval Sea Systems Command ATTN: SEA 62R SEA 64 Washington, DC 20362-5101
1	Commander Naval Air Systems Command ATTN: AIR-954-Tech Library Washington, DC 20360
4	Commander Naval Research Laboratory ATTN: Technical Library Code 4410, K. Kailasanate J. Boris E. Oran Washington, DC 20375-5000
1	Office of Naval Research ATTN: Code 473, R.S. Miller 800 N. Quincy Street Arlington, VA 22217-9999
1	Office of Naval Technology ATTN: ONT-213, D. Siegel 800 N. Quincy St. Arlington, VA 22217-5000

No. of Copies	Organization
4	Commander Naval Surface Warfare Center ATTN: Code 730 Code R-13, R. Bernecker H. Sandusky Silver Spring, MD 20903-5000
7	Commander Naval Surface Warfare Center ATTN: T.C. Smith K. Rice S. Mitchell S. Peters J. Consaga C. Gotzmer Technical Library Indian Head, MD 20640-5000
5	Commander Naval Surface Warfare Center ATTN: Code G30, Code G32, Code G33, J.L. East T. Doran Code E23 Technical Library Dahlgren, VA 22448-5000
5	Commander Naval Air Warfare Center ATTN: Code 388, C.F. Price T. Boggs Code 3895, T. Parr R. Derr Information Science Division China Lake, CA 93555-6001
2	Commanding Officer Naval Underwater Systems Center ATTN: Code 5B331, R.S. Lazar Technical Library Newport, RI 02840
1	AFOSR/NA ATTN: J. Tishkoff Bolling AFB, D.C. 20332-6448
1	OLAC PL/TSTL ATTN: D. Shiplett Edwards AFB, CA 93523-5000

No. of Copies	Organization
3	AL/LSCF ATTN: J. Levine L. Quinn T. Edwards Edwards AFB, CA 93523-5000
1	WL/MNAA ATTN: B. Simpson Eglin AFB, FL 32542-5434
1	WL/MNME Energetic Materials Branch 2306 Perimeter Rd. STE 9 Eglin AFB, FL 32542-5910
1	WL/MNSH ATTN: R. Drabczuk Eglin AFB, FL 32542-5434
2	NASA Langley Research Center ATTN: M.S. 408, W. Scallion D. Witcofski Hampton, VA 23605
1	Central Intelligence Agency Office of the Central References Dissemination Branch Room GE-47, HQS Washington, DC 20502
1	Central Intelligence Agency ATTN: J. Backofen HQ Room 5FL2 Washington, DC 20505
1	SDIO/TNI ATTN: L.H. Caveny Pentagon Washington, DC 20301-7100
1	SDIO/DA ATTN: E. Gerry Pentagon Washington, DC 21301-7100
2	HQ DNA ATTN: D. Lewis A. Fahey 6801 Telegraph Rd. Alexandria, VA 22310-3398

No. of Copies	Organization
1	Director Sandia National Laboratories Energetic Materials & Fluid Mechanics Department, 1512 ATTN: M. Baer P.O. Box 5800 Albuquerque, NM 87185
1	Director Sandia National Laboratories Combustion Research Facility ATTN: R. Carling Livermore, CA 94551-0469
4	Director Lawrence Livermore National Laboratory ATTN: L-355, A. Buckingham G. Benedetti M. Finger L-324, M. Constantino P.O. Box 808 Livermore, CA 94550-0622
2	Director Los Alamos Scientific Lab ATTN: T3/D. Butler M. Division/B. Craig P.O. Box 1663 Los Alamos, NM 87544
3	Battelle Columbus Laboratories ATTN: TACTEC Library, J.N. Huggins V. Levin 505 King Avenue Columbus, OH 43201-2693
1	Battelle PNL ATTN: Mr. Mark Garnich P.O. Box 999 Richland, WA 99352
1	Institute of Gas Technology ATTN: D. Gidaspow 3424 S. State Street Chicago, IL 60616-3896

No. of Copies	Organization
1	Institute for Advanced Technology ATTN: T.M. Krehne The University of Texas of Austin 4030-2 W. Braker Lane Austin, TX 78759-5329
2	CPIA - JHU ATTN: Hary J. Hoffman T. Christian 10630 Little Patuxent Parkway Suite 202 Columbia, MD 21044-3200
1	Brigham Young University Department of Chemical Engineering ATTN: M. Beckstead Provo, UT 84601
1	Jet Propulsion Laboratory California Institute of Technology ATTN: L.D. Strand, MS 125/224 4800 Oak Grove Drive Pasadena, CA 91109
1	California Institute of Technology 204 Karman Lab Main Stop 301-46 ATTN: F.E.C. Culick 1201 E. California Street Pasadena, CA 91109
3	Georgia Institute of Technology School of Aerospace Engineering ATTN: B.T. Zim E. Price W.C. Strahle Atlanta, GA 30332
1	Massachusetts Institute of Technology Department of Mechanical Engineering ATTN: T. Toong 77 Massachusetts Avenue Cambridge, MA 02139-4307
1	University of Illinois Department of Mechanical/Industry Engineering ATTN: H. Krier 144 MEB; 1206 N. Green St. Urbana, IL 61801-2978

No. of Copies	Organization
1	University of Maryland ATTN: Dr. J.D. Anderson College Park, MD 20740
1	University of Massachusetts Department of Mechanical Engineering ATTN: K. Jakus Amherst, MA 01002-0014
1	University of Minnesota Department of Mechanical Engineering ATTN: E. Fletcher Minneapolis, MN 55414-3368
3	Pennsylvania State University Department of Mechanical Engineering ATTN: V. Yang K. Kuo C. Merkle University Park, PA 16802-7501
1	Rensselaer Polytechnic Institute Department of Mathematics Troy, NY 12181
1	Stevens Institute of Technology Davidson Laboratory ATTN: R. McAlevy III Castle Point Station Hoboken, NJ 07030-5907
1	Rutgers University Department of Mechanical and Aerospace Engineering ATTN: S. Temkin University Heights Campus New Brunswick, NJ 08903
1	University of Southern California Mechanical Engineering Department ATTN: 0HE200, M. Gerstein Los Angeles, CA 90089-5199
1	University of Utah Department of Chemical Engineering ATTN: A. Baer Salt Lake City, UT 84112-1194
1	Washington State University Department of Mechanical Engineering ATTN: C.T. Crowe Pullman, WA 99163-5201

No. of Copies	Organization
1	AFELM, The Rand Corporation ATTN: Library D 1700 Main Street Santa Monica, CA 90401-3297
1	Arrow Technology Associates, Inc. ATTN: W. Hathaway P.O. Box 4218 South Burlington, VT 05401-0042
3	AAI Corporation ATTN: J. Hebert J. Frankle D. Cleveland P.O. Box 126 Hunt Valley, MD 21030-0126
2	Alliant Techsystems, Inc. ATTN: R.E. Tompkins J. Kennedy 7225 Northland Dr. Brooklyn Park, MN 55428
1	AVCO Everett Research Laboratory ATTN: D. Stickler 2385 Revere Beach Parkway Everett, MA 02149-5936
1	General Applied Sciences Lab ATTN: J. Erdos 77 Raynor Ave. Ronkonkama, NY 11779-6649
1	General Electric Company Tactical System Department ATTN: J. Mandzy 100 Plastics Ave. Pittsfield, MA 01201-3698
1	IITRI ATTN: M.J. Klein 10 W. 35th Street Chicago, IL 60616-3799
5	Hercules, Inc. Radford Army Ammunition Plant ATTN: D.A. Worrell W.J. Worrell R. Goft C. Chandler L. Rivenbark Radford, VA 24141-0299

No. of Copies	Organization
2	Hercules, Inc. Allegheny Ballistics Laboratory ATTN: William B. Walkup Thomas F. Farabaugh P.O. Box 210 Rocket Center, WV 26726
1	Hercules, Inc. Hercules Plaza ATTN: B.M. Riggleman Wilmington, DE 19894
1	MBR Research Inc. ATTN: Dr. Moshe Ben-Reuven 601 Ewing St., Suite C-22 Princeton, NJ 08540
1	Olin Corporation Badger Army Ammunition Plant ATTN: F.E. Wolf Baraboo, WI 53913
3	Olin Ordnance ATTN: E.J. Kirschke A.F. Gonzalez D.W. Worthington P.O. Box 222 St. Marks, FL 32355-0222
1	Olin Ordnance ATTN: H.A. McElroy 10101 9th Street, North St. Petersburg, FL 33716
1	Paul Gough Associates, Inc. ATTN: P.S. Gough 1048 South St. Portsmouth, NH 03801-5423
1	Physics International Library ATTN: H. Wayne Wampler P.O. Box 5010 San Leandro, CA 94577-0599
2	Princeton Combustion Research Laboratories, Inc. ATTN: N. Mer N.A. Messina Princeton Corporate Plaza 11 Deerpark Dr., Bldg IV, Suite 119 Monmouth Junction, NJ 08852

No. of Copies	Organization
3	Rockwell International Rocketdyne Division ATTN: BA08, J. Flanagan J. Gray R.B. Edelman 6633 Canoga Avenue Canoga Park, CA 91303-2703
2	Rockwell International Science Center ATTN: Dr. S. Chakravarthy Dr. S. Palaniswamy 1049 Camino Dos Rios P.O. Box 1085 Thousand Oaks, CA 91360
1	Southwest Research Institute ATTN: J.P. Riegel 6220 Culebra Road P.O. Drawer 28510 San Antonio, TX 78228-0510
1	Sverdrup Technology, Inc. ATTN: Dr. John Deur 2001 Aerospace Parkway Brook Park, OH 44142
2	Thiokol Corporation Elkton Division ATTN: R. Biddle Tech Library P.O. Box 241 Elkton, MD 21921-0241
1	Veritay Technology, Inc. ATTN: E. Fisher 4845 Millersport Hwy. East Amherst, NY 14501-0305
1	Universal Propulsion Company ATTN: H.J. McSpadden 25401 North Central Ave. Phoenix, AZ 85027-7837
1	SRI International Propulsion Sciences Division ATTN: Tech Library 333 Ravenwood Avenue Menlo Park, CA 94025-3493

No. of Copies	Organization
	Aberdeen Proving Ground
1	Cdr, USACSTA ATTN: STECS PO/R. Hendricksen

No. of Copies	Organization
1	Ernst-Mach-Institut ATTN: Dr. R. Heiser Haupstrasse 18 Weil am Rheim Germany
1	Defence Research Agency, Military Division ATTN: C. Woodley RARDE Fort Halstead Sevenoaks, Kent, TN14 7BP England
1	School of Mechanical, Materials, and Civil Engineering ATTN: Dr. Bryan Lawton Royal Military College of Science Shrivenham, Swindon, Wiltshire, SN6 8LA England
2	Institut Saint Louis ATTN: Dr. Marc Giraud Dr. Gunther Sheets Postfach 1260 7858 Weail am Rhein 1 Germany

No. of Copies	Organization
1	Explosive Ordnance Division ATTN: A. Wildegger-Gaissmaier Defence Science and Technology Organisation P.O. Box 1750 Salisbury, South Australia 5108
1	Armaments Division ATTN: Dr. J. Lavigne Defence Research Establishment Valcartier 2459, Pie XI Blvd., North P.O. Box 8800 Courcelette, Quebec G0A 1R0 Canada
1	U.S. Army European Research Office ATTN: Dr. Roy E. Richenbach Box 65 FPO New York 09510-1500

INTENTIONALLY LEFT BLANK.

USER EVALUATION SHEET/CHANGE OF ADDRESS

This Laboratory undertakes a continuing effort to improve the quality of the reports it publishes. Your comments/answers to the items/questions below will aid us in our efforts.

1. ARL Report Number ARL-TR-77 ____________ Date of Report February 1993 ____________

2. Date Report Received ____

3. Does this report satisfy a need? (Comment on purpose, related project, or other area of interest for which the report will be used.) ____

____

____

4. Specifically, how is the report being used? (Information source, design data, procedure, source of ideas, etc.) ____

____

____

5. Has the information in this report led to any quantitative savings as far as man-hours or dollars saved, operating costs avoided, or efficiencies achieved, etc? If so, please elaborate. ____________

____

____

6. General Comments. What do you think should be changed to improve future reports? (Indicate changes to organization, technical content, format, etc.) ____

____

____

____

CURRENT ADDRESS

____
Organization

____
Name

____
Street or P.O. Box No.

____
City, State, Zip Code

7. If indicating a Change of Address or Address Correction, please provide the Current or Correct address above and the Old or Incorrect address below.

OLD ADDRESS

____
Organization

____
Name

____
Street or P.O. Box No.

____
City, State, Zip Code

(Remove this sheet, fold as indicated, staple or tape closed, and mail.)

DEPARTMENT OF THE ARMY

OFFICIAL BUSINESS

BUSINESS REPLY MAIL
FIRST CLASS PERMIT No 0001, APG, MD

Postage will be paid by addressee

NO POSTAGE
NECESSARY
IF MAILED
IN THE
UNITED STATES

Director
U.S. Army Research Laboratory
ATTN: AMSRL-OP-CI-B (Tech Lib)
Aberdeen Proving Ground, MD 21005-5066